Current **A**pplied **S**cience and **T**echnology e-ISSN: 2586-9396

Curr. Appl. Sci. Technol. ….., Vol... (No...), e0270271

Research article

Fabrication of g-C_3N_4 Nanosheets Through Solvent-Assisted Synthesis for Improved Photocatalytic Applications

Htet Yadanar Soe[1], Thanate Na Wichean[2], Gasidit Panomsuwan[1], Oratai Jongprateep[1] and Ratchatee Techapiesancharoenkij[1]*

[1]Special Research Unit for Biomass Conversion Technology for Energy and Environment, Department of Materials Engineering, Faculty of Engineering, Kasetsart University, 50 Ngam Wong Wan Rd, Ladyao Chatuchak, Bangkok 10900, Thailand
[2]Materials Innovation Center, Faculty of Engineering, Kasetsart University, 50 Ngam Wong Wan Rd. Ladyao Chatuchak, Bangkok 10900, Thailand

Received:22 December 2025, Revised: 6 June 2026, Accepted: 10 June 2026, Published: 20 July 2026

Abstract

Graphitic carbon nitride (g-C_3N_4) has emerged as a photocatalyst material of interest due to its strong visible-light activity, good stability, and tunable electronic properties, making it attractive for environmental and energy-related applications. However, producing high quality exfoliated g-C_3N_4 nanosheets using a simple and low-cost technique remains challenging. In this work, bulk g-C_3N_4 was synthesized through the thermal polymerization of melamine and subsequently exfoliated ultrasonically in either deionized water (CN-DI) or isopropanol (CN-IPA). Different exfoliation pathways including thermal, chemical, and one-step methods were examined to determine their impact on the nanosheets' structural and photocatalytic characteristics. X-ray diffraction (XRD) confirmed that the crystalline structure of g-C_3N_4 remained intact after exfoliation. Transmission electron microscopy (TEM) and scanning electron microscope (SEM) analyses showed the formation of ultrathin nanosheet-like structures with a layered morphology. The ultrathin nanosheets displayed broadened interlayer spacing, as further supported by UV-Vis and photoluminescence (PL) results that showed a noticeable red shift, enhanced light absorption, and reduced electron-hole recombination in CN-DI and CN-IPA compared with bulk g-C_3N_4. These improvements primarily stem from increased surface area, better charge separation, and more effective photon utilization achieved through ultrasonic exfoliation. Photocatalytic tests additionally revealed that both CN-DI and CN-IPA achieved more than 60% degradation of organic dyes under UV illumination. Overall, the findings highlight a straightforward, green, and scalable approach for producing high-performance g-C_3N_4 nanosheets suitable for wastewater purification under UV-light environment.

Keywords: g-C_3N_4 nanosheets; thermal polymerization; ultrasonic exfoliation; photocatalytic activity

*Corresponding author: E-mail: fengrct@ku.ac.th
https://doi.org/10.55003/cast.2026.270271

1. Introduction

The rapid growth of industrial activities has led to the excessive use of synthetic dyes in numerous manufacturing sectors, including textiles, paper, leather, pharmaceuticals, and cosmetics (Ardila-Leal et al., 2021). Among these, methylene blue (MB) is frequently used because it is inexpensive, chemically stable, and produces strong coloration. However, the direct discharge of MB and similar dyes into natural water systems severely impacts environmental quality and human health. Dye effluents reduce light penetration, disturb photosynthetic activity in aquatic ecosystems, and contain toxic, mutagenic, and carcinogenic compounds (Rubio et al., 2025). Prolonged exposure to such pollutants has been associated with respiratory irritation, dermatitis, and allergic reactions (Sun et al., 2016). Furthermore, the aromatic molecular structures of synthetic dyes make them resistant to biological degradation, resulting in long-term persistence in aquatic environments (Mabuza et al., 2023).To address dye pollution, several treatment strategies have been developed, including adsorption (Crini, 2006), membrane filtration (Rashidi et al., 2015),electrochemical oxidation (Brillas & Martínez-Huitle, 2015), and chemical coagulation have been developed to remove dyes from wastewater (Robinson et al., 2001). However, these approaches generally transfer the contaminants to another phase instead of fully decomposing them. In contrast, photocatalytic degradation offers a sustainable and efficient solution by using semiconductor materials to generate reactive species that convert complex organic pollutants into harmless products like carbon dioxide and water (Dassanayake et al., 2021). TiO_2 photocatalysts have gained wide attention, but their limited visible-light activity has driven efforts to improve their efficiency and modified systems such as WO_3-coated TiO_2 nanotubes and immobilized TiO_2 in CPC reactors show enhanced charge separation and photocatalytic performance (Chuenkruit et al., 2025). Visible-light-active materials like Co-doped TiO_2 further expand photocatalytic capabilities, enabling effective degradation of commercial dyes (Noonuruk & Wattanawikkam, 2019). As a result, photocatalysis continues to attract attention for environmental purification and renewable-energy-related applications.

Graphitic carbon nitride (g-C_3N_4) has become an attractive photocatalyst material due to its suitable band gap (~2.7 eV), strong visible-light absorption, and overall structural stability (Wang et al., 2008). Since its introduction as a photocatalyst in 2006, g-C_3N_4 has been extensively applied in hydrogen production, CO_2 reduction, and the degradation of organic contaminants (Fan et al., 2025). Nevertheless, pristine bulk g-C_3N_4 suffers from several drawbacks, including limited surface exposure, fast electron-hole recombination, and limited light absorption, which restrict its photocatalytic efficiency (Ismael, 2020). To address these limitations, several modification approaches have been investigated, such as atomic doping, heterojunction interface engineering, and material morphology tuning (Xu et al., 2024). Notably, converting g-C_3N_4 into two-dimensional (2D) nanosheets has been especially effective, as the exfoliation process increases surface area, exposes additional active sites, and enhances charge-transport pathways, thereby boosting photocatalytic performance (Yang et al., 2013). Different exfoliation techniques have been investigated to improve the morphological framework and optical behavior of g-C_3N_4 nanosheets. Thermal exfoliation involves high-temperature oxidation to remove surface layers and generate porous structures, enhancing light absorption and surface reactivity (Tong et al., 2015b; Soe et al., 2026). Chemical exfoliation, often carried out using oxidizing acids such as H_2SO_4 or HNO_3, can produce thinner nanosheets but may introduce chemical defects and structural damage (Sun et al., 2017). Ultrasonic exfoliation breaks weak interlayer van der Waals interactions through acoustic cavitation, producing uniform

nanosheets without substantial chemical alteration (Ma et al., 2016). Additionally, one-step exfoliation methods, such as the direct calcination of precursors with gas-releasing agents (NH_4Cl or citric acid), have been developed to achieve simultaneous polymerization and exfoliation (Wang et al., 2019). Although all these techniques can successfully yield exfoliated g-C_3N_4, the resulting structural and photocatalytic properties vary significantly. Ultrasonic-assisted exfoliation is particularly attractive due to its simplicity, environmental friendliness, and preservation of the g-C_3N_4 framework, often enhancing photocatalytic efficiency under visible-light irradiation (Zhang et al., 2016). Ultrasonic exfoliation has been widely used to produce thin nanosheets of graphitic carbon nitride (g-C_3N_4) with improved surface area and photocatalytic performance. However, most previous studies have primarily employed ultrasonic bath systems and have focused on single-solvent exfoliation processes. The influence of different solvents on the exfoliation efficiency and resulting physicochemical properties of g-C_3N_4 nanosheets has not been systematically investigated.

In this study, DI water and isopropanol (IPA) were used as exfoliation solvents to examine the influence of solvent properties on the delamination of bulk g-C_3N_4. DI water provides good dispersion due to its high polarity, while IPA, with lower surface tension, can more easily penetrate between stacked layers. Comparing these two solvents helps clarify how solvent selection affects the formation of nanosheets and the photocatalytic properties of the nanosheets. The choice of solvent significantly influences the exfoliation behavior of g-C_3N_4. Polar solvents help separate interlayer sheets effectively, while organic solvents enhance dispersion and limit restacking. The synthesized nanosheets were characterized using X-ray diffraction (XRD), transmission electron microscopy (TEM), UV-Vis absorption, and photoluminescence (PL) spectroscopy. Photocatalytic performance was assessed through the UV irradiation degradation of methylene blue. Overall, this study offers a facile, environmentally friendly strategy for producing high-performance g-C_3N_4 nanosheets and provides valuable insight into how solvent-assisted ultrasonic exfoliation enhances charge separation and photocatalytic efficiency, supporting the design of sustainable photocatalysts for water purification under UV-light environment.

2. Materials and Methods

Melamine (99%) was sourced from SIGMA Co., Ltd. (Germany). Isopropanol (≥99.7 wt.%) was obtained from LOBA Chemie Laboratory Reagent & Fine Chemicals Co., Ltd. (India), and methylene blue (MB) was purchased from KOSDAQ Co., Ltd. (Korea). All chemicals used in this study were of analytical grade. Deionized water was utilized in all experimental procedures.

2.1 Bulk g-C_3N_4 preparation procedure

Bulk g-C_3N_4 was produced by heating melamine to induce thermal decomposition. In this process, 15 g of melamine was placed inside a covered ceramic crucible and heated at a rate of 5°C min^{-1} until reaching 560°C, where the temperature was held for 5 h under ambient conditions. During calcination, melamine undergoes polymerization, releasing ammonia and forming graphitic carbon nitride (Molaei & Rahimi, 2021).

$$3C_3H_6N_6(s) \longrightarrow 3\ g\text{-}C_3N_4\ (s) + 6NH_3(g) \quad (1)$$

After heating, the crucible was left to cool naturally to room temperature. The resulting yellow solid was then crushed and ground to a fine powder using a mortar and pestle to yield bulk g-C_3N_4. This powder served as the precursor for subsequent ultrasonic-assisted exfoliation. Deionized water (DI) and isopropanol (IPA) were used as solvents to prepare both bulk g-C_3N_4 and exfoliated g-C_3N_4 nanosheets. Depending on the solvent, oxidation-assisted exfoliation produced two types of nanosheets: CN-DI and CN-IPA.

2.2 Dispersion and solvent-assisted exfoliation of g-C_3N_4

For the exfoliation step, as shown in Figure 1, 100 mg of bulk g-C_3N_4 was dispersed in 100 mL of DI water or IPA. Ultrasonic treatment promoted the separation of g-C_3N_4 layers within the suspension. The mixture was sonicated using an ultrasonic homogenizer (BEM-650A, 220V, 50 Hz) at 40% amplitude for 3h. The suspension was centrifuged using a centrifuge (DM0412-50, Ponpe Instrument, China) at 3000 rpm for 10 min. The resulting 2D g-C_3N_4 nanosheets were collected from the supernatant and used as the exfoliated samples.

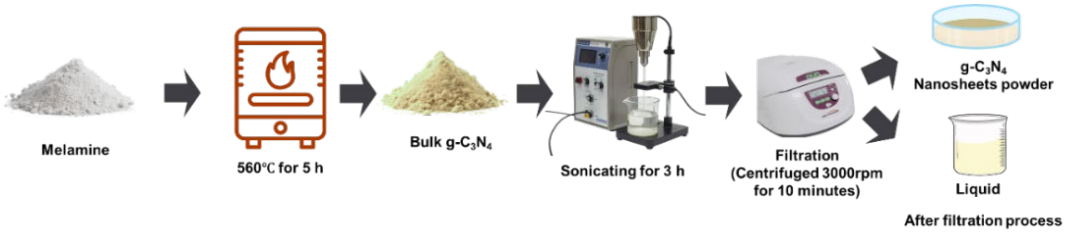

Figure 1. Schematic representation of the preparation for exfoliated g-C_3N_4 nanosheets

2.3 Characterization

The crystal structures of the synthesized samples were characterized using a Philips X'Pert X-ray diffractometer equipped with a Cu Kα radiation source (λ = 0.154 nm), operated at 40 kV and 30 mA, across a 2θ range of 10-50°. The scans were performed at a rate of 0.02° s^{-1}. Crystallite sizes were estimated using the Scherrer equation (Villalobos et al., 2020).

$$D = 0.89\lambda/(\beta\cos\theta) \quad (2)$$

where θ is the Bragg diffraction angle, λ is the X-ray wavelength, and β represents the full width at half maximum (FWHM). Fourier-transform infrared (FTIR) spectra were recorded at room temperature using a KBr pellet technique, covering the 400-4000 cm^{-1} range with a Bruker Alpha-E spectrometer. Transmission electron microscopy (TEM) was employed to investigate the morphological and structural characteristics of the samples, using a JEOL JEM-3010F operated at 300 kV. UV-Vis absorption spectra were collected using a SHIMADZU UV-1700 spectrophotometer for the 200–800 nm spectrum range. The powder samples were dispersed in IPA solvents for the UV-Vis absorption measurement. Tauc plots were constructed to determine the optical bandgap, assuming a direct bandgap semiconductor (Yang et al., 2017).

$$\alpha h\nu = (h\nu - E_g)^{1/2} \quad (3)$$

where α, h, ν, E_g represent the absorption coefficient, Plank's constant, the photon frequency, and the energy band gap, respectively. Photoluminescence (PL) spectra were recorded with a HORIBA fluorescence spectrophotometer at an excitation wavelength of 350 nm.

2.4 Evaluation of methylene blue photodegradation

The photocatalytic behavior of bulk g-C_3N_4, CN-DI, and CN-IPA nanosheets was evaluated by monitoring their ability to degrade methylene blue (MB) in aqueous solution. The MB solution was irradiated using a 365 nm UV lamp (UVGL-58) with an intensity of 1.5 mW cm^{-2} at a distance of 15 cm. For each experiment, 0.05 g of catalyst was added to 100 mL of a 10 mg L^{-1} MB solution in a glass beaker. The mixture was stirred in the dark for one hour to establish adsorption-desorption equilibrium before irradiation with UV light.

During UV-Vis light exposure, 3 mL of the suspension was collected every 15 min, immediately filtered to remove the catalyst, and analyzed using a UV-Vis spectrophotometer to quantify the remaining concentration of MB. The degradation efficiency was determined using the equation:

$$\%R = \left(\frac{C_0 - C_t}{C_0}\right) \times 100 \quad (4)$$

where *%R* is the removal percentage, C_0 is the initial dye concentration, and C_t is the concentration at time t.

To analyze the degradation kinetics, $\ln(C/C_0)$ was plotted against irradiation time (t), where C_0 represents the initial dye concentration and C_0 corresponds to the concentration at a given time. The linear relationship obtained from this plot suggests that the degradation process follows a pseudo–first-order kinetic model:

$$\ln(C/C_0) = k\,t \quad (5)$$

where *k* is the apparent rate constant (min^{-1}). The pseudo first-order behavior indicates that the degradation rate mainly depends on the dye concentration, rather than involving simultaneous interactions among multiple reactants as in second-order reactions. Such kinetic behavior is commonly observed in photocatalytic systems, where the degradation of organic dyes is primarily driven by reactive species generated on the catalyst surface, including hydroxyl radicals (•OH) and superoxide radicals (O_2•$^-$), which promote the breakdown of dye molecules (Tsaviv et al., 2024).

3. Results and Discussion

3.1 Structure characterization

The XRD patterns of the synthesized g-C_3N_4 materials provide information on the structural modifications induced by solvent-assisted treatment with deionized water (DI) and isopropanol (IPA), as shown in Figure 2. In agreement with previous reports, the diffraction peaks at approximately 27.1° and 13.1° correspond to the (002) and (100) planes of

graphitic carbon nitride, respectively (Thomas et al., 2008). The peak near 12.5° reflects the in-plane structural repetition of the tri-s-triazine units, while the strong peak around 27.5° originates from the stacking of aromatic layers associated with the (002) plane (Li et al., 2021b).

The full width at half maximum (FWHM) of the (002) diffraction peak varies among the samples, indicating differences in crystallite size. As summarized in Table 1, the bulk g-C_3N_4 displays a larger crystallite size than the CN-DI and CN-IPA nanosheets based on the Scherrer equation. These variations result from distinct exfoliation behaviors: solvent-assisted treatment promotes layer separation, yielding smaller crystallites and confirming the successful formation of g-C_3N_4 nanosheets. Furthermore, DI and IPA assisted treatments reduce the crystallinity of the bulk material and disrupt its long-range atomic ordering. This structural modification is evident from the weakened diffraction intensities of both characteristic peaks in the treated samples.

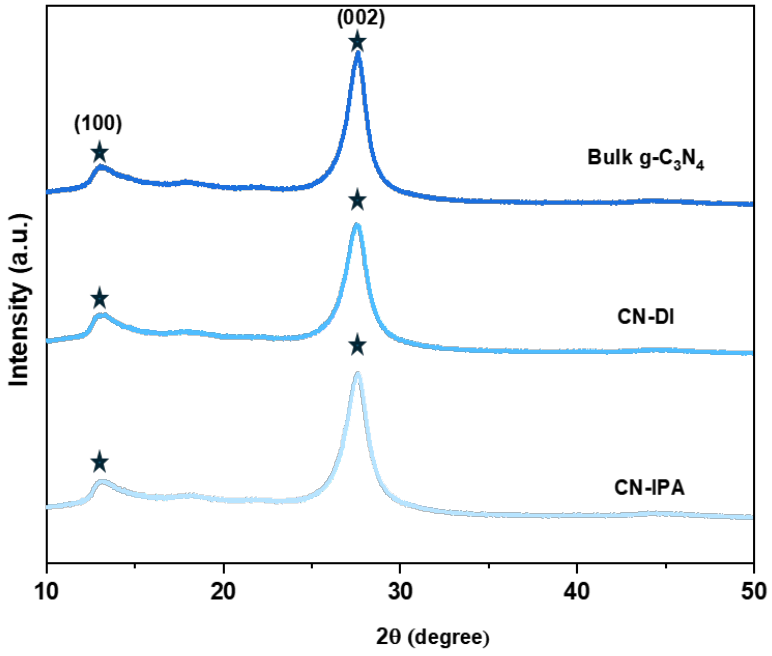

Figure 2. XRD results of bulk g-C_3N_4, exfoliated CN-DI, and CN-IPA nanosheets.

Table 1. Crystallite sizes of the g-c_3n_4-based photocatalysts calculated using the Scherrer equation.

Sample	Crystallize Size(nm)
Bulk g-C_3N_4	48
CN-DI	43
CN-IPA	41

3.2 Phase structure

FTIR analysis was performed in the 400-4000 cm^{-1} region to investigate the chemical structures of bulk g-C_3N_4 and the exfoliated CN-DI and CN-IPA nanosheets (Figure 3). The wide absorption band observed around 3000-3600 cm^{-1} corresponds to N-H stretching vibrations (Duan et al., 2015; Schwinghammer et al., 2014). Characteristic C-N heterocycle vibrations are found between 1200 and 1700 cm^{-1}, while the bending mode of the triazine ring occurs near 810 cm^{-1}, in agreement with earlier studies on g-C_3N_4 (Han et al., 2016). The triazine-related peaks in CN-DI and CN-IPA display lower intensity compared to the bulk material, indicating that solvent-assisted exfoliation disrupts the ordered stacking of structural motifs. Moreover, samples treated with DI and IPA exhibit a noticeably broader band around 3200-3600 cm^{-1}, which originates from the stretching vibrations of -N-H and -O-H groups introduced during the exfoliation process and isopropanol (IPA) results in neither elemental doping (Dong et al., 2014) nor the formation of a heterojunction (Dong et al., 2013) in the final product.

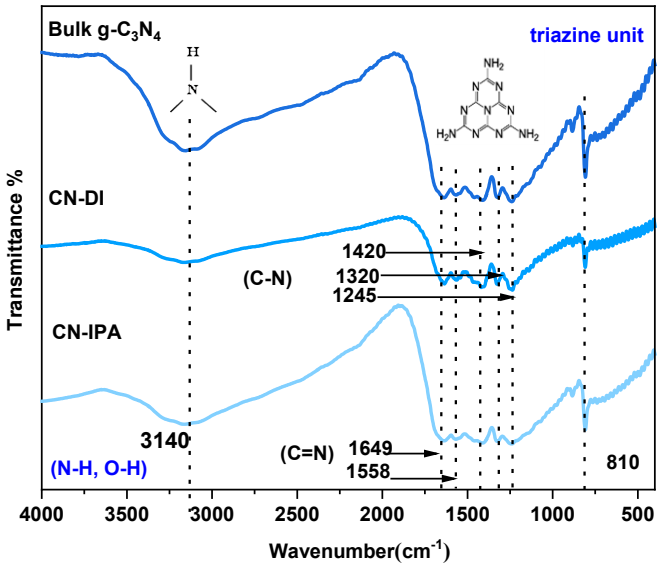

Figure 3. FTIR spectra of bulk g-C_3N_4, exfoliated CN-DI and CN-IPA nanosheets

3.3 BET surface areas

To determine the surface area of the g-C_3N_4 materials, nitrogen adsorption-desorption experiments were analyzed. The patterns in Figure 4 reveal that all thermally exfoliated g-C_3N_4 samples exhibit type-IV isotherms based on the BDDT classification, along with H_3-type hysteresis loops defined by IUPAC. This indicates the presence of slit-like mesoporous structures. The bulk g-C_3N_4 showed a surface area of 5 m^2/g, whereas the CN-DI and CN-IPA samples showed increased values of 32 m^2/g and 49 m^2/g, respectively. This enhanced porosity and surface area in the exfoliated samples contribute to their improved catalytic performance by providing more active sites and facilitating mass transport (Beyhaqi et al., 2021).

3.4 Morphology

The morphological characteristics of the bulk g-C_3N_4 and the exfoliated nanosheets (CN-DI and CN-IPA) were investigated through scanning electron microscopy (SEM) and transmission electron microscopy (TEM), as illustrated in Figures 5 and 6. The bulk g-C_3N_4 (Figure 5a) presents a compact and tightly layered architecture, which is typical of materials synthesized via the thermal polymerization of melamine. Its closely stacked layers reduce the number of exposed active sites and restrict charge migration, leading to relatively weak photocatalytic behavior (Linh et al., 2021).

In contrast, the exfoliated nanosheets (Figures 5b and 5c) display a more open and fragmented morphology, with thinner sheets and irregular edges. The CN-DI sample shows partially separated layers and a rougher surface texture, while the CN-IPA nanosheets exhibit improved delamination and a more porous appearance. These morphological features indicate successful exfoliation and greater exposure of reactive sites, which can facilitate enhanced photocatalytic activity (Chen et al., 2023).

TEM images (Figure 6) reveal clear structural differences among the samples. Bulk g-C_3N_4 (Figure 6a) exhibits densely stacked layers with strong contrast, indicating a compact multilayer structure with limited electron transparency. In comparison, CN-DI (Figure 6b) displays partially exfoliated nanosheets with increased transparency, suggesting a more loosely stacked layered structure, although some aggregation remains. The CN-IPA sample (Figure 6c) shows highly transparent and wrinkled nanosheets, which are characteristic of well-exfoliated few-layer structures with significantly reduced stacking. These observations suggest that the exfoliation process is more effective in CN-IPA, resulting in thinner and more dispersed nanosheets compared with bulk g-C_3N_4 and CN-DI.

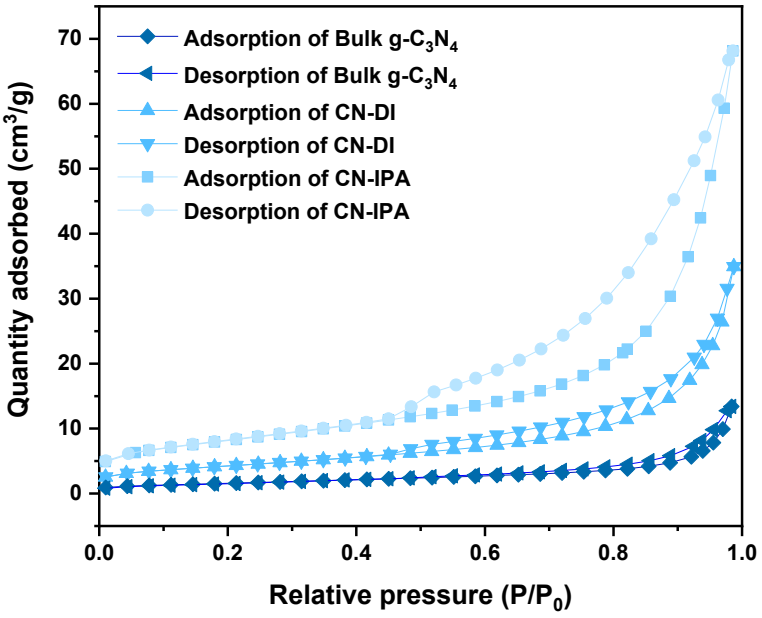

Figure 4. BET results of bulk g-C_3N_4, exfoliated CN-DI and CN-IPA nanosheets

Table 2. Surface area for bulk g-C_3N_4, CN-DI and CN-IPA nanosheets

Sample	Surface Area (m^2/g)
Bulk g-C_3N_4	5
CN-DI	32
CN-IPA	49

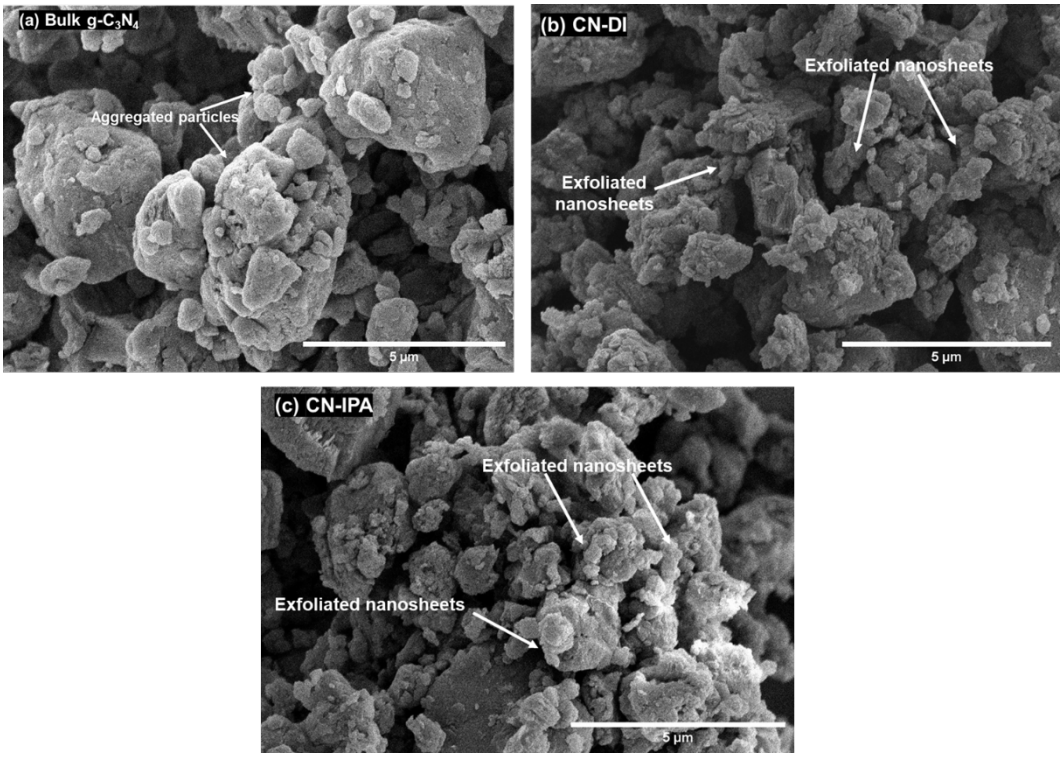

Figure 5. SEM results of (a) bulk g-C_3N_4 (b) exfoliated CN-DI and (c) CN-IPA nanosheets

The more effective exfoliation observed for CN-IPA can be attributed to the solvent properties of isopropanol. Compared with DI water, IPA possesses lower surface tension and moderate polarity, which facilitates the penetration of solvent molecules between the stacked layers of bulk g-C_3N_4 during ultrasonication. This interaction weakens the van der Waals forces between adjacent layers and promotes their separation into thinner nanosheets. In addition, IPA can provide better dispersion stability and enhance cavitation effects during ultrasonic treatment, further assisting the delamination process (Sun et al., 2017). These observations suggest that the exfoliation process is more effective in CN-IPA, resulting in thinner and more dispersed nanosheets compared with bulk g-C_3N_4 and CN-DI.

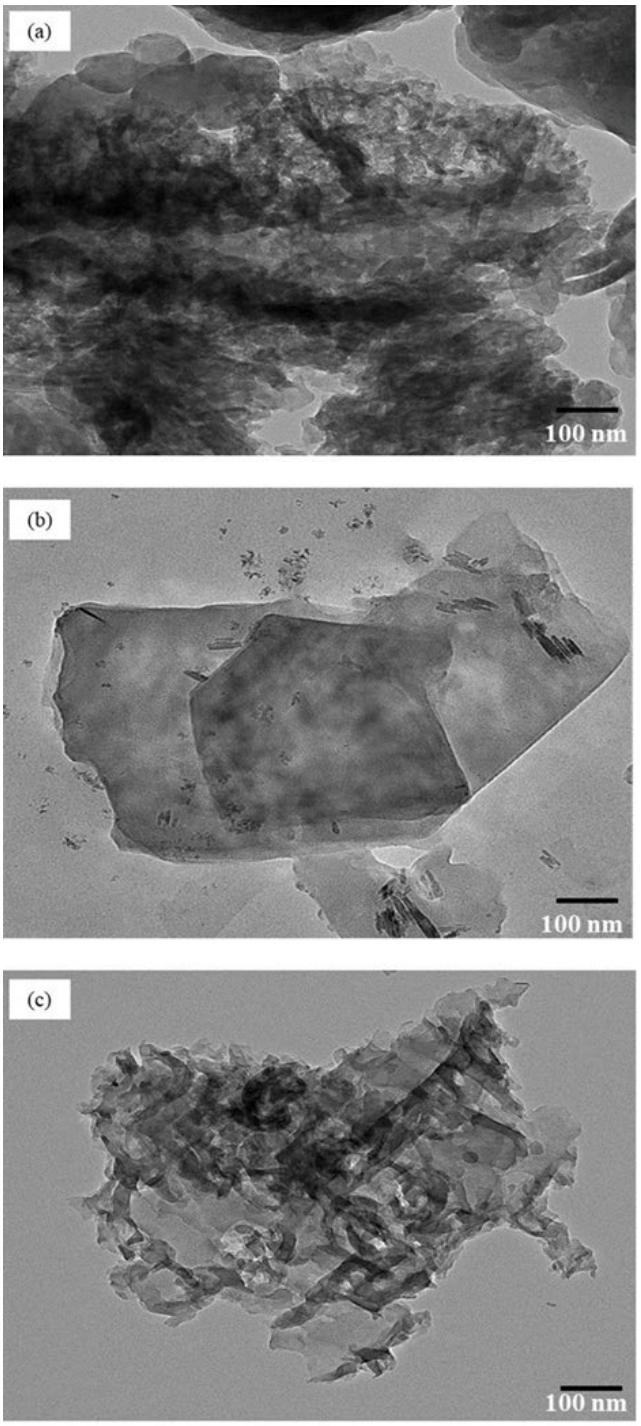

Figure 6. TEM results of (a) bulk g-C_3N_4 (b) exfoliated CN-DI and (c) CN-IPA nanosheets

3.5 Optical properties

UV-Vis absorption and photoluminescence (PL) analyses were performed to investigate the optical behavior of the bulk g-C_3N_4 and the exfoliated CN-DI and CN-IPA nanosheets, as shown in Figures 7 and 8, respectively. In Figure 7a, the exfoliated nanosheets exhibit enhanced absorption intensity in the blue-green region (450-550 nm) compared with bulk g-C_3N_4. This increased absorption in the visible region suggests improved light-harvesting capability after exfoliation, which is beneficial for photocatalytic applications. Notably, the absorption edge positions of CN-DI and CN-IPA remain close to that of bulk g-C_3N_4, indicating that the intrinsic band gap is only slightly affected by the exfoliation process. The Tauc plot (Figure 7b) shows the tailing edge of the nanosheets, which is slightly displaced to the visible region at lower energy. The calculated bandgaps for CN-DI and CN-IPA nanosheets are 2.80 and 2.75, respectively, while that of bulk g-C_3N_4 is 2.65 eV, in good agreement with previously reported values (Wang et al., 2008).

The photoluminescence (PL) spectra of the bulk g-C_3N_4 and exfoliated CN-DI and CN-IPA nanosheets under 375 nm excitation exhibit a strong intrinsic emission band peaking at around 470 nm, attributed to direct electron-hole recombination near the band transition. This emission intensity correlates with the efficiency of separating and recombining photogenerated charge carriers in photocatalysts, reflecting their optical and electronic properties. Compared with bulk g-C_3N_4, the exfoliated CN-IPA nanosheets show a slight blue shift of the emission peak, which can be attributed to the thinner nanosheet structure and quantum confinement effect after exfoliation. In contrast, CN-DI exhibits a slight red shift, possibly due to surface defects or structural changes introduced during the exfoliation process, which benefits photocatalytic performance (Yan et al., 2012).

Overall, the UV-Vis and PL results indicate that the CN-DI and CN-IPA nanosheets exhibit significantly enhanced photocatalytic behavior compared with bulk g-C_3N_4. The improved performance can be attributed to the broader visible light absorption and more efficient charge separation observed in the exfoliated samples. In addition, exfoliation typically increases the specific surface area of g-C_3N_4 nanosheets, thereby providing a larger number of exposed reactive sites for photocatalytic reactions. Previous studies have reported that the surface area of exfoliated g-C_3N_4 can increase several times compared with bulk materials, which significantly enhances photocatalytic activity. Moreover, the lower PL intensity observed for CN-DI and CN-IPA suggests suppressed recombination of photogenerated electron-hole pairs, indicating more efficient charge carrier migration (Sun et al., 2017; Palanivel et al., 2025). These combined structural and electronic improvements promote effective light absorption, charge separation, and surface reaction processes, leading to superior photocatalytic performance of the exfoliated samples.

3.6 Photocatalytic degradation performance

In Figure 9, the UV-Vis spectra show a gradual decline in the characteristic absorption peak of methylene blue (MB) at approximately 664 nm as irradiation time increases, confirming the effective photodegradation of MB by the g-C_3N_4-based catalysts. The MB peak intensity steadily decreases from 0 to 60 min for all samples, indicating continuous photocatalytic breakdown of the dye under UV illumination. For bulk g-C_3N_4 (Figure 9a), the reduction in absorbance is relatively small, suggesting limited photocatalytic activity. In comparison, the CN-DI (Figure 9b) and CN-IPA (Figure 9c) samples show a more noticeable decrease in peak intensity, confirming that the exfoliation treatment enhances the photocatalytic performance. Figure 10 further illustrates the degradation behavior of the samples. As

shown in Figure 10a, the C/C_0 value continuously decreases with irradiation time for all catalysts, with CN-IPA exhibiting the most rapid decline, followed by CN-DI and bulk g-C_3N_4. The corresponding degradation efficiencies after 60 min are summarized in Figure 10b, where bulk g-C_3N_4 achieves 31% degradation, while CN-DI and CN-IPA reach 45% and 62%, respectively.

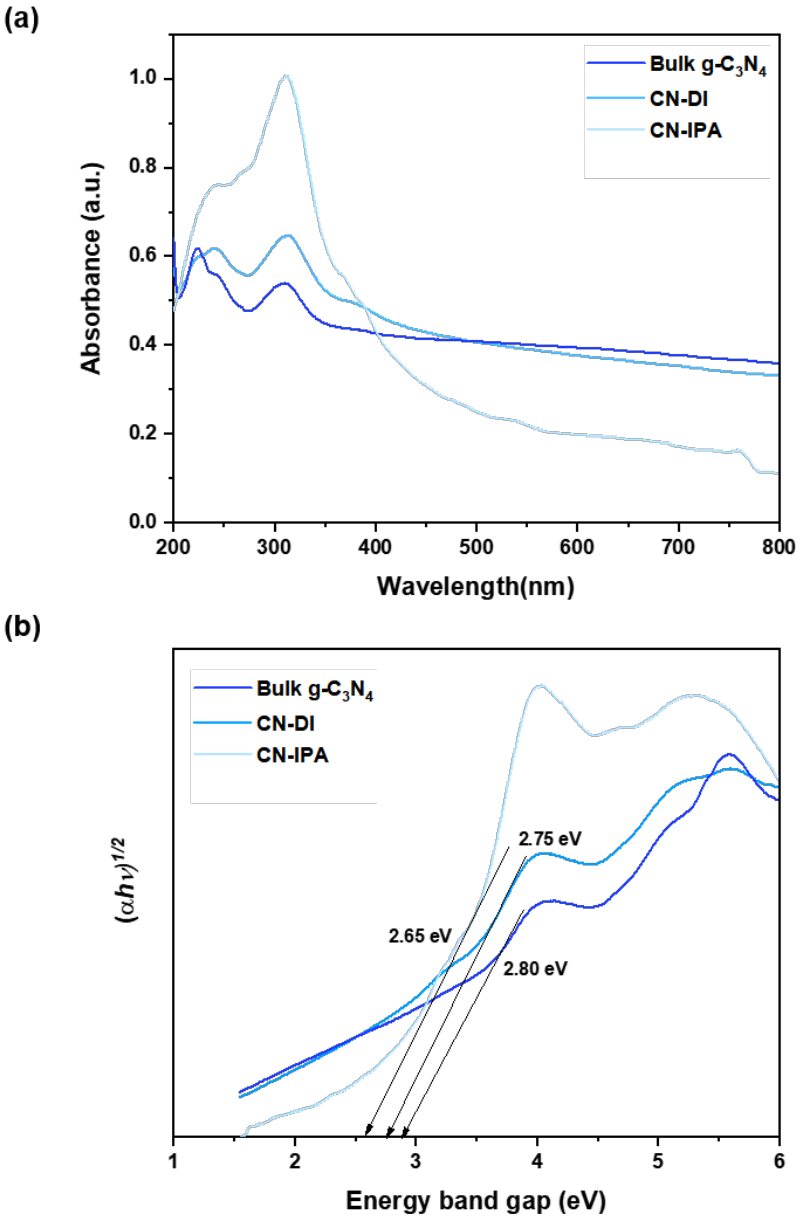

Figure 7. (a) UV absorbance spectra and (b) Tauc plots of bulk g-C_3N_4, exfoliated CN-DI and CN-IPA nanosheets

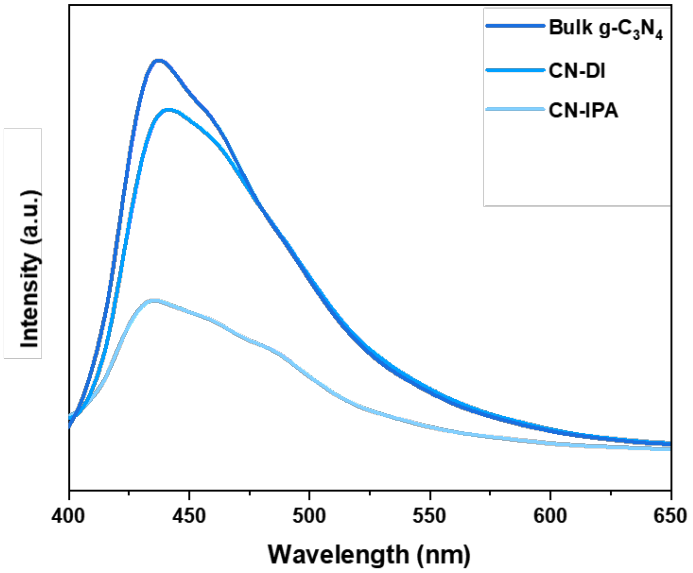

Figure 8. Photoluminescence (PL) spectra of bulk g-C_3N_4, exfoliated CN-DI and CN-IPA nanosheets

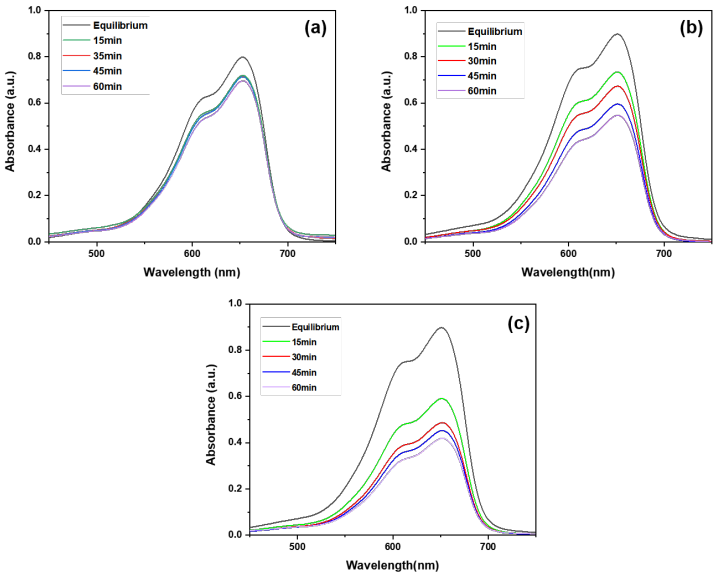

Figure 9. Time-dependent absorption spectra of MB aqueous solution degradation by (a) bulk g-C_3N_4, (b) exfoliated CN-DI, and (c) CN-IPA nanosheets under UV illumination

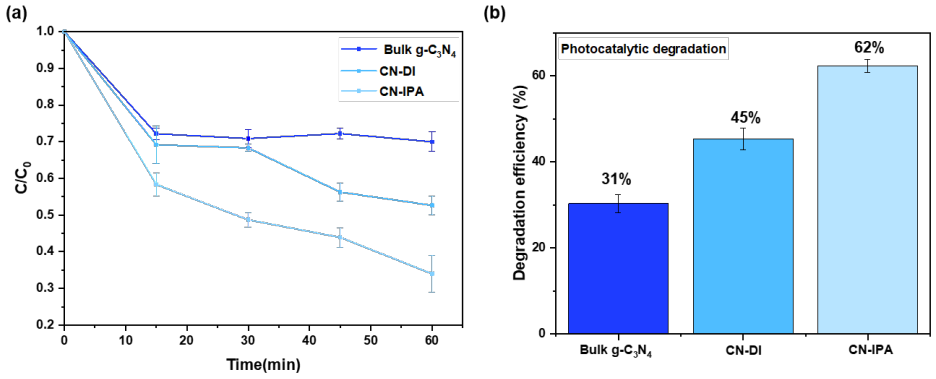

Figure 10. Degradation of MB aqueous solution by bulk g-C_3N_4, exfoliated CN-DI, and CN-IPA nanosheets under UV illumination: (a) the the C/C_0 value of MB aqueous solution over irradiation time, and (b) the degradation efficiency after 60 min of irradiation

The photocatalytic degradation kinetics were examined using a pseudo-first-order kinetic model based on the Langmuir-Hinshelwood approach shown in Figure 11. The plots of $\ln(C_0/C_t)$ versus irradiation time displayed a good linear relationship for all samples, confirming that the degradation reaction follows pseudo-first-order behavior. The rate constant k increases from 0.005 min^{-1} for bulk g-C_3N_4 to 0.009 min^{-1} for CN-DI and 0.014 min^{-1} for CN-IPA. Notably, the CN-IPA sample exhibited the highest apparent rate constant, indicating improved photocatalytic efficiency relative to CN-DI and bulk g-C_3N_4. The enhanced activity of the IPA-assisted nanosheets can be attributed to their larger accessible surface area, improved dispersion, and better separation of photogenerated electron-hole pairs. These advantages likely stem from residual organic groups introduced during IPA treatment. After 60 min of UV light exposure, bulk g-C_3N_4 showed significantly lower MB degradation than CN-DI and CN-IPA, and its performance was even lower than some previously reported liquid-exfoliated nanosheets(Huanxin et al., 2014; Tong et al., 2015a). Both CN-DI and CN-IPA exhibit markedly faster reaction rates than bulk g-C_3N_4, highlighting the advantages conferred by their nanosheet architectures. The increased porosity and reduced layer thickness of these materials promote more efficient charge transport and facilitate the generation of reactive oxygen species, thereby accelerating MB oxidation. These improvements are closely associated with the enlarged specific surface area of the nanosheet structures, which supports effective charge-carrier separation and suppresses recombination. The higher surface area further strengthens the interaction between reactant molecules and the catalyst surface, promoting improved adsorption and subsequent photocatalytic steps. In addition, the porous nanosheet framework enables smoother charge transfer, minimizes recombination losses, and facilitates electron migration from the bulk to the surface, enhancing interactions with adsorbed MB molecules. The results confirm that solvent-assisted exfoliation greatly improves the photocatalytic behavior of g-C_3N_4. Isopropanol (IPA) demonstrates more effective exfoliation due to its suitable solvent properties. Its moderate polarity and relatively low surface tension improve the dispersion of g-C_3N_4 layers and allow the solvent to more easily penetrate between the stacked sheets. Moreover, during ultrasonication, IPA can intensify cavitation phenomena, producing stronger shear forces that assist in separating the layers and lead to the formation of thinner nanosheets. Among all tested samples, the CN-IPA nanosheets exhibit

the highest efficiency in UV irradiation induced degradation of methylene blue, highlighting their strong potential as a promising photocatalyst for wastewater-treatment application.

The photocatalytic efficiency of the synthesized samples, their performance was compared with previously reported g-C_3N_4 nanosheet-based photocatalysts. The comparison is summarized in Table 3.

Table 3 compares the photocatalytic degradation of methylene blue (MB) using different g-C_3N_4 materials reported in the literature. Bulk g-C_3N_4 generally shows low photocatalytic efficiency (~21%) due to its limited surface area and rapid recombination of photogenerated electron–hole pairs. Structural modifications such as exfoliation or ball-milling significantly improve photocatalytic performance by increasing the exposed active sites and facilitating charge transfer, under UV irradiation. In this work, the CN-IPA sample exhibited 62% MB degradation within 60 min under UV light, which is considerably higher than bulk g-C_3N_4. This improvement can be attributed to the formation of thinner layered structures that enhance the availability of active sites and promote photocatalytic reactions.

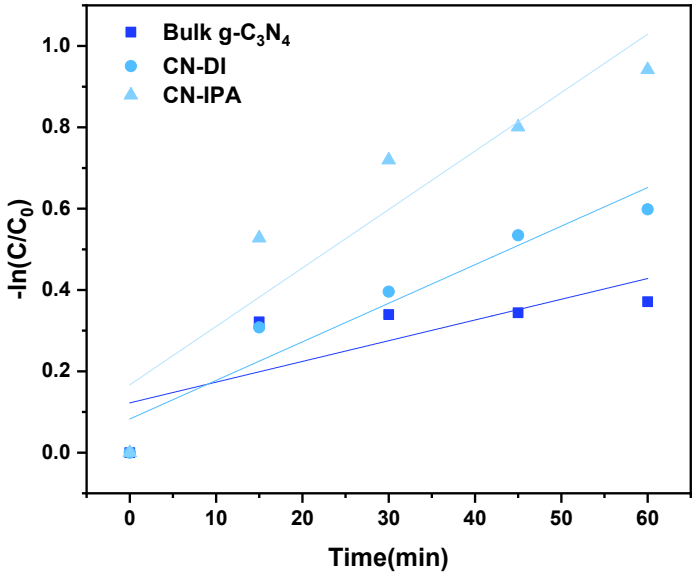

Figure 11. The first-order kinetic plots of methylene blue (MB) photodegradation over bulk g-C_3N_4, exfoliated CN-DI and CN-IPA nanosheet under UV illumination

3.7 Reusability and stability of the photocatalyst

The reusability of the prepared scaffolds was evaluated to assess their potential for practical dye removal applications. After each cycle, the photocatalyst was recovered from the reaction suspension by centrifugation at 4500 rpm for 10 min for 5 times. The collected solid was washed several times with ethanol and deionized water to remove residual MB molecules and reaction intermediates adsorbed on the catalyst surface. Subsequently, the sample was further rinsed with ethanol to eliminate any remaining organic impurities. The washed catalyst was then dried in an oven at 60°C for 12 h before being reused in the photocatalytic cycle. This washing and drying procedure was repeated after each cycle to ensure the stability and reusability of the photocatalyst, as presented in Figure 12.

The results demonstrate that the catalyst maintains relatively high activity during repeated cycles, although a slight decline in performance is gradually observed. The dye removal efficiency decreases from about 62% in the first cycle to 60% in the second cycle and further to 55% in the third cycle. This slight reduction in activity is likely associated with the accumulation of residual dye species on the catalyst surface, which may block some active sites and limit light absorption, thereby affecting the generation and transport of photoinduced charge carriers.

Table 3. Photocatalytic performance comparison of g-C_3N_4 nanosheet photocatalysts reported in previous studies

No	Material	Pollutant	Light Source	Time	MB Degradation	Ref
1	Pure g-C_3N_4	MB	UV-Vis	30 min	~21%	(Qiu & Li, 2024)
2	Sulfuric acid-treated g-C_3N_4 nanosheets	MB	Sunlight irradiation	180 min	~ 93.12 %	(Solayman et al., 2024)
3	Exfoliated g-C_3N_4	RhB	Light irradiation	60 min	~ 93.5 %	(Amiri et al., 2023)
4	Tubular g-C_3N_4 structure	MB	Visible light	180 min	~98%	(Li et al., 2021a)
5	CN-DI	MB	UV	60 min	~45%	This work
6	CN-IPA	MB	UV	60 min	~62%	This work

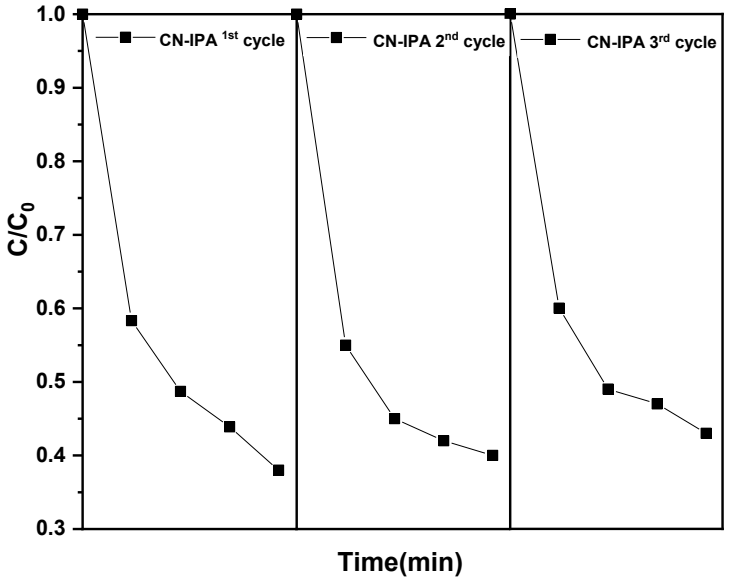

Figure 12. Photocatalytic reusability performance of the CN-IPA sample over three consecutive degradation cycles

4. Conclusions

In conclusion, we effectively produced 2D g-C_3N_4 nanosheets using the liquid exfoliation approach. The current exfoliation method is straightforward and time-saving because it involves mixing calcined g-C_3N_4 with either IPA or DI water solvents followed by sonication. Incorporating DI and IPA into the exfoliation process imparts distinctive properties to the g-C_3N_4 nanosheets, including an appropriate band gap energy and efficient electron-hole pair recombination. The distinctive properties of g-C_3N_4 nanosheets contribute to their exceptional photocatalytic performance. This research shows an understanding of this method of exfoliating polymeric materials into nanosheets. The rate at which MB degrades on g-C_3N_4 nanosheets exceeds that on bulk g-C_3N_4. The porous structure of g-C_3N_4 nanosheets produced with solvents provides their improved photocatalytic performance. However, additional optimization may be required to improve performance even further. The photocatalytic properties significantly improved due to greater separation efficiency of photo-excited carriers and improved light harvesting from the larger available specific surface area. Thus, the excellent photocatalytic activity shows that these materials have a promising future as high-performance photocatalysts for addressing global environmental and energy challenges.

5. Acknowledgements

This research was supported by the Faculty of Engineering, Kasetsart University for the international Ph.D. scholarship. HYS thanks AUN/SEED-Net, JICA for student support. Kasetsart University Research and Development Institute is acknowledged for the support of the Special Research Unit for Biomass Conversion Technology for Energy and Environment, KURDI Grant No. FF(KU) 51.67.

6. Authors' Contributions

Htet Yadanar Soe: Conceptualization, Methodology, Investigation, Data curation, Formal analysis, Writing Original draft preparation, Reviewing and Editing.
Thanate Na Wichean: Methodology, Formal analysis.
Gasidit Panomsuwan: Funding acquisition, Supervision, Methodology.
Oratai Jongprateep: Conceptualization, Funding acquisition, Supervision, Methodology.
Ratchatee Techapiesancharoenkij: Conceptualization, Funding acquisition, Supervision, Resources, Methodology, Formal analysis, Reviewing and Editing, Correspondence.

ORCID
Htet Yadanar Soe https://orcid.org/0009-0003-8028-7629
Thanate Na Wichean https://orcid.org/0000-0003-4439-8885
Gasidit Panomsuwan https://orcid.org/0000-0003-4316-5035
Oratai Jongprateep https://orcid.org/0000-0001-5160-5091
Ratchatee Techapiesancharoenkij https://orcid.org/0000-0002-6026-7685

7. Conflicts of Interest

The authors declare no conflict of interest.

8. AI Declaration

The authors declare that Large Language Models (LLMs) were used solely to improve language clarity and correct grammar errors. The manuscript was reviewed and edited by the authors. The authors take full responsibility for the content of this publication. No generative AI tools were used for purposes other than those stated above.

References

Amiri, S., Yazdani, F., & Mortaheb, H. (2023). Exfoliated graphitic carbon nitride nanosheets for visible light photocatalytic degradation of Rhodamine B - Investigation on exfoliation method. *Materials Chemistry and Physics*, *301*, Article 127623. https://doi.org/10.1016/j.matchemphys.2023.127623

Ardila-Leal, L. D., Poutou-Piñales, R. A., Pedroza-Rodríguez, A. M., & Quevedo-Hidalgo, B. E. (2021). A brief history of colour, the environmental impact of synthetic dyes and removal by using laccases. *Molecules*, *26*(13), Article 3813. https://doi.org/10.3390/molecules26133813

Beyhaqi, A., Azimi, S. M. T., Chen, Z., Hu, C., & Zeng, Q. (2021). Exfoliated and plicated g-C_3N_4 nanosheets for efficient photocatalytic organic degradation and hydrogen evolution. *International Journal of Hydrogen Energy*, *46*(39), 20547-20559. https://doi.org/10.1016/j.ijhydene.2021.03.174

Brillas, E., & Martínez-Huitle, C. A. (2015). Decontamination of wastewaters containing synthetic organic dyes by electrochemical methods. An updated review. *Applied Catalysis B: Environment and Energy*, *166-167*, 603-643. https://doi.org/ 10.1016/j.apcatb.2014.11.016

Chen, L., Maigbay, M., Li, M., & Qiu, X. (2023). Synthesis and modification strategies of g-C_3N_4 nanosheets for photocatalytic applications. *Advanced Powder Materials*, *3*, Article 100150. https://doi.org/10.1016/j.apmate.2023.100150

Chuenkruit, A., Thongjoon, W., Aiempanakit, M., Aiempanakit, C., & Aiempanakit, K. (2025). Preparation of WO_3 on TiO_2 nanotubes for electrochromic-enhanced photocatalytic activity. *Current Applied Science and Technology*, *25*(5), Article e0263966. https://doi.org/10.55003/cast.2025.263966

Crini, G. (2006). Non-conventional low-cost adsorbents for dye removal: A review. *Bioresource Technology*, *97*(9), 1061-1085. https://doi.org/10.1016/j.biortech.2005.05.001

Dassanayake, R. S., Acharya, S., & Abidi, N. (2021). Recent advances in biopolymer-based dye removal technologies. *Molecules*, *26*(15), Article 4697. https://doi.org/10.3390/molecules26154697

Dong, F., Zhao, Z., Xiong, T., Ni, Z., Zhang, W., Sun, Y., & Ho, W. (2013). In situ construction of g-C_3N_4/g-C_3N_4 metal-free heterojunction for enhanced visible-light photocatalysis. *ACS Applied Materials and Interfaces*, *5*, 113922-11401. https://doi.org/10.1021/am403653a

Dong, G., Ai, Z., & Zhang, L. (2014). Efficient anoxic pollutant removal with oxygen functionalized graphitic carbon nitride under visible light. *RSC Advances*, *4*(11), 5553-5560. https://doi.org/10.1039/c3ra46068a

Duan, J., Chen, S., Jaroniec, M., & Qiao, S. Z. (2015). Porous C_3N_4 nanolayers@N-graphene films as catalyst electrodes for highly efficient hydrogen evolution. *ACS Nano*, *9*(1), 931-940. https://doi.org/10.1021/nn506701x

Fan, Y., Chang, X., Wang, W., & Fan, H. (2025). Graphitic carbon nitride for photocatalytic hydrogen production from water splitting: Nano-morphological control and electronic

band tailoring. *Nanomaterials*, *15*(1), Article 45. https://doi.org/10.3390/nano15010045

Han, Q., Wang, B., Gao, J., Cheng, Z., Zhao, Y., Zhang, Z., & Qu, L. (2016). Atomically thin mesoporous nanomesh of graphitic C_3N_4 for high-efficiency photocatalytic hydrogen evolution. *ACS Nano*, *10*(2), 2745-2771. https://doi.org/10.1021/acsnano.5b07831

Huanxin, Z., Yu, H., Quan, X., Chen, S., Zhao, H., & Wang, H. (2014). Atomic single layer graphitic-C_3N_4: Fabrication and its high photocatalytic performance under visible light irradiation. *RSC Advance*, *4*(2), 624-628. https://doi.org/10.1039/C3RA45776A

Ismael, M. (2020). A review on graphitic carbon nitride (g-C_3N_4) based nanocomposites: Synthesis, categories, and their application in photocatalysis. *Journal of Alloys and Compounds*, *846*, Article 156446. https://doi.org/10.1016/j.jallcom.2020.156446

Li, H., Zang, L., Shen, F., Wang, L., Sun, L., & Yuan, F. (2021a). Tubular g-C_3N_4/carbon framework for high-efficiency photocatalytic degradation of methylene blue. *RSC Advances*, *11*(30), 18519-18524. https://doi.org/10.1039/d1RA02918e

Li, J., Wang, Y., Li, X., Gao, Q., & Zhang, S. (2021b). A facile synthesis of high-crystalline g-C_3N_4 nanosheets with closed self-assembly strategy for enhanced photocatalytic H_2 evolution. *Journal of Alloys and Compounds*, *881*, Article 160551. https://doi.org/10.1016/j.jallcom.2021.160551

Linh, P. H., Do Chung, P., Van Khien, N., Oanh, L. T. M., Thu, V. T., Bach, T. N., Hang, L. T., Hung, N. M., & Lam, V. D. (2021). A simple approach for controlling the morphology of g-C_3N_4 nanosheets with enhanced photocatalytic properties. *Diamond and Related Materials*, *111*, Article 108214. https://doi.org/10.1016/j.diamond.2020.108214

Ma, T., Bai, J., Liang, H., Wang, J., & Li, C. (2016). An efficient method for assembling layered g-C_3N_4 nanosheets grow on 1D pore channels carbon fibers as a composite photocatalyst by ultrasound-assisted exfoliation and hydrothermal method. *Vacuum*, *134*, 130-135. https://doi.org/10.1016/j.vacuum.2016.10.013

Mabuza, L., Sonnenberg, N., & Marx-Pienaar, N. (2023). Natural versus synthetic dyes: Consumers' understanding of apparel coloration and their willingness to adopt sustainable alternatives. *Resources, Conservation and Recycling Advances*, *18*, Article 200146. https://doi.org/10.1016/j.rcradv.2023.200146

Molaei, P., & Rahimi-Moghadam, F. (2021). Porous g-C_3N_4 nanosheets through facile thermal polymerization of melamine in the air for photocatalyst application. *Journal of Materials Science: Materials in Electronics*, *32*, 19655-19666. https://doi.org/10.1007/s10854-021-06488-z

Noonuruk, R., & Wattanawikkam, C. (2019). Visible-light-driven photodegradation of commercial dyes by the cooperation of co-doped TiO_2 material. *Current Applied Science and Technology*, *20*(1), 43-51.

Palanivel, B., Theras, J. E. M., Dhas, S. S. J., Dhas, S. A. M. B., Oh, T. H., Sangaraju, S., Alsaeedi, H., & Vignesh, S. (2025). Shock wave-induced exfoliated g-C_3N_4 nanosheets for an enhanced visible-light-driven photocatalytic activity. *Diamond and Related Materials*, *152*, Article 111911. https://doi.org/10.1016/j.diamond.2024.111911

Qiu, S., & Li, J. (2024). High-efficiency ag-modified ZnO/g-C_3N_4 photocatalyst with 1D-0D-2D morphology for methylene blue degradation. *Molecules*, *29*(10), Article 2182. https://doi.org/10.3390/molecules29102182

Rashidi, H. R., Sulaiman, N. M. N., Hashim, N. A., Hassan, C. R. C., & Ramli, M. R. (2015). Synthetic reactive dye wastewater treatment by using nano-membrane filtration. *Desalination and Water Treatment*, *55*(1), 86-95. https://doi.org/10.1080/19443994.2014.912964

Robinson, T., McMullan, G., Marchant, R., & Nigam, P. (2001). Remediation of dyes in textile effluent: a critical review on current treatment technologies with a proposed

alternative. *Bioresource Technology*, *77*(3), 247-255. https://doi.org/10.1016/S0960-8524(00)00080-8

Rubio, F. T. V., Maciel, G. M., Bortolini, D. G., Fernandes, I. D. A. A., Pedro, A. C., Ribeiro, I. S., Fávaro-Trindade, C. S., Peralta, R. M., & Haminiuk, C. W. I. (2025). Artificial dyes: Health risks, environmental concerns, and the rise of natural alternatives. *Trends in Food Science and Technology*, *162*, Article 105085. https://doi.org/10.1016/j.tifs.2025.105085

Schwinghammer, K., Mesch, M. B., Duppel, V., Ziegler, C., Senker, J., & Lotsch, B. V. (2014). Crystalline carbon nitride nanosheets for improved visible-light hydrogen evolution. *Journal of the American Chemical Society*, *136*(5), 1730-1733. https://doi.org/10.1021/ja411321s

Solayman, H. M., Yahya, N. Y., Leong, K. H., Hossain, M. K., Kang, K., Sim, L. C., Zoh, K.-D., Khan, M. B., & Aziz, A. A. (2024). Photocatalytic performance of acid exfoliated graphitic carbon nitride (g-C_3N_4) for the degradation of dye under direct sunlight. *FlatChem*, *48*, Article 100762. https://doi.org/10.1016/j.flatc.2024.100762

Soe, H. Y., Na Wichean, T., Panomsuwan, G., Jongprateep, O., & Techapiesancharoenkij, R. (2026). 3D-printed polymeric resin composites with g-C_3N_4 nanosheets for efficient dye removal in wastewater treatment. *Chiang Mai Journal of Science, 53*(2), Article e2026032. https://doi.org/10.12982/CMJS.2026.032

Sun, H., Zhou, X., Zhang, H., & Tu, W. (2017). An efficient exfoliation method to obtain graphitic carbon nitride nanosheets with superior visible-light photocatalytic activity. *International Journal of Hydrogen Energy*, *42*(12), 7930-7937. https://doi.org/10.1016/j.ijhydene.2016.12.080

Sun, S., Xie, S., Chen, H., Cheng, Y., Shi, Y., Qin, X., Dai, S. Y., Zhang, X., & Yuan, J. S. (2016). Genomic and molecular mechanisms for efficient biodegradation of aromatic dye. *Journal of Hazardous Materials*, *302*, 286-295. https://doi.org/10.1016/j.jhazmat.2015.09.071

Thomas, A., Fischer, A., Goettmann, F., Antonietti, M., Müller, J.-O., Schlögl, R., & Carlsson, J. M. (2008). Graphitic carbon nitride materials: variation of structure and morphology and their use as metal-free catalysts. *Journal of Materials Chemistry, 18*(41)*, 4893-4908*. https://doi.org/10.1039/B800274F

Tong, J., Zhang, L., Li, F., Li, M., & Cao, S. (2015a). An efficient top-down approach for the fabrication of large-aspect-ratio g-C_3N_4 nanosheets with enhanced photocatalytic activities. *Physical Chemistry Chemical Physics*, *17*(36), 23532-23537. https://doi.org/10.1039/c5cp04057d

Tong, J., Zhang, L., Li, F., Wang, K., Han, L., & Cao, S. (2015b). Rapid and high-yield production of g-C_3N_4 nanosheets via chemical exfoliation for photocatalytic H_2 evolution. *RSC Advances*, *5*(107), 88149-88153. https://doi.org/10.1039/C5RA16988G

Tsaviv, J. N., Eneji, I. S., Shato'Ato, R., Ahemen, I., Jubu, P., & Yusof, Y. (2024). Photodegradation, kinetics and non-linear error functions of methylene blue dye using $SrZrO_3$ perovskite photocatalyst. *Heliyon*, *10*(14), Article e34517. https://doi.org/10.1016/j.heliyon.2024.e34517

Villalobos, L. F., Vahdat, M., Dakhchoune, M., Nadizadeh, Z., Mensi, M., Oveisi, E., Campi, D., Marzari, N., & Agrawal, K. V. (2020). Large-scale synthesis of crystalline g-C_3N_4 nanosheets and high-temperature H_2 sieving from assembled films. *Science Advances*, *6*(4), Article eaay9851. https://doi.org/10.1126/sciadv.aay9851

Wang, L., Hou, Y., Xiao, S., Bi, F., Zhao, L., Li, Y., Zhang, X., Gai, G., & Dong, X. (2019). One-step, high-yield synthesis of g-C_3N_4 nanosheets for enhanced visible light photocatalytic activity. *RSC Advances*, *9*(67), 39304-39314. https://doi.org/10.1039/C9RA08922E

Wang, X., Maeda, K., Thomas, A., Takanabe, K., Xin, G., Carlsson, J., Domen, K., & Antonietti, M. (2008). A metal-free polymeric photocatalyst for hydrogen production from water under visible light. *Nature Materials*, *8*, 76-80. https://doi.org/10.1038/nmat2317

Xu, X., Huang, Z., Tan, L., Zhang, Z., Chen, B., Xia, X., Cheng, G., & Chen, X. (2024). Surface modification of g-C_3N_4 for enhanced photocatalytic activity via a simple illumination in pure water. *Applied Surface Science*, *672*, Article 160794. https://doi.org/10.1016/j.apsusc.2024.160794

Yan, H., Chen, Y., & Xu, S. (2012). Synthesis of graphitic carbon nitride by directly heating sulfuric acid treated melamine for enhanced photocatalytic H_2 production from water under visible light. *International Journal of Hydrogen Energy*, *37*(1), 125-133. https://doi.org/10.1016/j.ijhydene.2011.09.072

Yang, S., Gong, Y., Zhang, J., Zhan, L., Ma, L., Fang, Z., Vajtai, R., Wang, X., & Ajayan, P. M. (2013). Exfoliated graphitic carbon nitride nanosheets as efficient catalysts for hydrogen evolution under visible light. *Advanced Materials*, *25*(17), 2452-2456. https://doi.org/10.1002/adma.201204453

Yang, Y., Chen, J., Mao, Z., An, N., Wang, D., & Fahlman, B. D. (2017). Ultrathin g-C_3N_4 nanosheets with an extended visible-light-responsive range for significant enhancement of photocatalysis. *RSC Advances*, *7*, 2333-2341. https://doi.org/10.1039/C6RA26172H

Zhang, L., Huang, F., Liang, C., Zhou, L., Zhang, X., & Pang, Q. (2016). Ultrasound exfoliation of g-C_3N_4 with assistance of cadmium ions and synthesis of CdS/g-C_3N_4 ultrathin nanosheets with efficient photocatalytic activity. *Journal of the Taiwan Institute of Chemical Engineers*, *60*, 643-650. https://doi.org/10.1016/j.jtice.2015.11.013